Beyond the harmonic approximation description of wobbling excitations in even-even nuclei with frozen alignments

R. Budaca [1,2,*] and C. M. Petrache[3]

[1] *"Horia Hulubei" National Institute for Physics and Nuclear Engineering, Str. Reactorului 30, RO-077125, POB-MG6 Bucharest-Măgurele, Romania*

[2] *Academy of Romanian Scientists, Splaiul Independenţei 54, 050044 Bucharest, Romania*

[3] *Université Paris-Saclay, CNRS/IN2P3, IJCLab, 91405 Orsay, France*

(Received 21 March 2022; accepted 14 July 2022; published 21 July 2022)

The wobbling motion in even-even nuclei is investigated by means of a collective Hamiltonian constructed from a semiclassical treatment applied to a triaxial rotor with a rigidly aligned pair of quasiparticles. The limits of distinct wobbling regimes are discussed in connection to the dynamic evolution of the wobbling excitations and corresponding electromagnetic properties. Model calculations are performed for the description of transverse wobbling bands in ^{130}Ba, ^{134}Ce, and ^{136,138}Nd nuclei.

DOI: 10.1103/PhysRevC.106.014313

I. INTRODUCTION

Nuclear wobbling excitation is a unique feature of triaxial nuclei. It arises as a consequence of the comparable distribution of mass and, respectively, of moments of inertia (MOI) along the body fixed principal axes. Despite favoring rotation around the intrinsic axis with maximal MOI, a triaxial rigid body will have a more complex motion with precession and nutation components inferred by the strong rotational contribution from the other axes. Initially, Davydov and Filipov [1] showed that the low lying collective states in some nuclei can be described by the eigenvalues of a triaxial rigid rotor Hamiltonian. In what concerns wobbling motion, it was first suggested by Bohr and Mottelson [2] as a possible manifestation in even-even nuclei at high spin, providing thus a phenomenological interpretation for the excited states of the triaxial rigid body Hamiltonian [3]. Unfortunately, the envisaged purely collective wobbling in even-even nuclei cannot be sustained because of the low-frequency breaking of nucleon pairs by the Coriolis force. However, the presence of an odd nucleon blocks the first low-frequency pair breaking mechanism, while its angular momentum alignment facilitates the rigid triaxiality of the core [4]. This phenomenon was confirmed by the properties of the strongly deformed bands based on an aligned $i_{13/2}$ proton, observed in the ^{161,163,165,167}Lu [5–8] and ^{167}Ta [9] nuclei.

The more complex particle-rotor system leads to a few distinct types of wobbling motions. The longitudinal wobbling refers to the rotation around the axis with the maximal MOI and the alignment of the single-particle spin along the same axis [10,11]. It is the particle-rotor counterpart of the originally proposed wobbling mechanism [2]. The alignment of the single-particle spin along a principal axis which is perpendicular to the axis with the maximal MOI, enhances the dynamical MOI along the corresponding axis. This effect decreases with increasing total angular momentum, up to a critical angular momentum where the effective dynamical MOI along the alignment axis is counterbalanced by the maximal MOI of the triaxial rigid core. Before this critical point, the system's rotation commences along an axis which is perpendicular to the body fixed axis with maximal MOI, and the associated dynamical mode is called transverse wobbling [10,11]. After the critical angular momentum, the rotation axis starts to tilt towards the body fixed axis with maximal MOI. This tilted-axis dynamical mode is not yet well understood.

The main tool for the study and interpretation of the wobbling excitations is the particle-rotor model (PRM) [2,11–20], whose quantum structure allows the systematization of discrete states in terms of total angular momentum and one of its projections which is a good quantum number. The drawback of this description is the lack of information regarding the dynamics of the system which is usually described with classical concepts. Moreover, the PRM Hamiltonian is usually diagonalized in a strong coupling basis [2], where the separation and interplay of the single-particle and the rotor degrees of freedom are not obvious. Second hand dynamical information can be extracted by means of quantum averages or semiclassical mappings [12,17–20]. Alternatively, the tilted axis cranking (TAC) approaches based on the mean field theory [21], provide a direct relation between the density distribution and the total angular momentum direction [11,22], but due to its semiclassical nature cannot describe consistently the quantum interaction between microscopic configurations. Beyond the mean field ventures based on random phase approximation (RPA) [23–28], collective Hamiltonian [29–31] or angular momentum projection techniques [32–36] are presently employed in order to incorporate the quantum correlations in the cranking mean field solutions.

*Corresponding author: rbudaca@theory.nipne.ro

All wobbling bands observed in $A \approx 160$ region exhibit a longitudinal alignment [12,13]. Recently, these bands have been instead interpreted as transverse wobbling bands, under the hypothesis of a frozen orthogonal geometry of the angular momenta of the unpaired nucleon and the core, even though the bands are observed up to very high spin where the Coriolis force imposes the parallel geometry [11]. Transverse wobbling in odd-even nuclei has been recently proposed additionally at low spin in ^{135}Pr [22,34], ^{105}Pd [37], and ^{183}Au [38]. There are also some reports of longitudinal wobbling in ^{133}La [39], ^{187}Au [40], and ^{127}Xe [41]. The wobbling character of these low-spin bands is however strongly questioned due to the inadequacy of the wobbling harmonic approximation at low spins [3,14,15,42], and the contradictory experimental data regarding either predominant $E2$ or $M1$ nature of the interband transitions. In this context, alternative interpretations were put forward, such as the tilted precession mode [42,43], or the consistent accounting for the γ-softness within the interacting boson fermion model description of Nomura and Petrache [44]. On the other hand, in order to contemplate a wobbling phenomenology at low spins, a consistent treatment of anharmonicities is needed.

Wobbling in even-even nuclei is possible in the mainframe of the same blocking mechanism of the pair breaking which can be realized with two-quasiparticle configurations. Such bands based on the $\pi h_{11/2}^2$ configuration have been recently identified and discussed in ^{130}Ba [35,45,46] and ^{136}Nd [36,47,48] nuclei. Also the neighboring ^{134}Ce and ^{138}Nd nuclei exhibit bands with similar properties which hint at a wobbling interpretation [48–50]. A $\nu h_{11/2}^{-2}$ band was also observed in ^{138}Nd which is a candidate for the novel wobbling generated by hole alignments [50].

In order to investigate the wobbling dynamics in such bands, we perform here a semiclassical analysis on a system composed of a triaxial core and a rigidly aligned pair of quasiparticles. For a quantitative description of the wobbling bands from the four considered nuclei, we constructed a quantum Hamiltonian with a consistent accounting for anharmonic effects. As all past semiclassical approaches to wobbling excitation were always limited to the harmonic approximation [11,51–57], this represents the main theoretical novelty of the study. The solutions of the quantum Hamiltonian are used to reproduce the experimental energy levels and the associated electromagnetic properties, offering thus information regarding the deformation and dynamics of the considered nuclei.

II. THEORETICAL FORMALISM

In what follows one will consider that the spins of the quasiparticles are all rigidly aligned to one of the principal axes of the intrinsic frame of reference. Let us denote the resultant spin of the quasiparticles by $\vec{j}$. For a pair of quasiparticles in the $h_{11/2}$ orbital, this amounts to $|\vec{j}| = 10$. This assumption is consistent with the angular momentum distribution for a set of particles in an intruder orbital, which has a sharp maximum in the maximally allowed value [58]. The interaction between the two quasiparticles is neglected, due to the stability of the pair configuration attested for example in backbending phenomena [59]. Then the rigid or frozen alignment (FA) is expressed as $\hat{j}_a \approx j \equiv \text{const}$ and $\hat{j}_{k\neq a} = 0$, where a denotes the alignment principal axis. With this approximation, the relevant part of the particle-rotor Hamiltonian [2] is reduced to

$$H_{\text{align}} = H_I - H_{Ij}^a \tag{2.1}$$

with

$$H_I = \sum_{k=1}^{3} A_k \hat{I}_k^2, \quad H_{Ij}^a = 2A_a j \hat{I}_a, \quad a = 1, 2, 3, \tag{2.2}$$

where $A_i = 1/(2\mathcal{J}_i)$. Here, we employ hydrodynamic moments of inertia [2]:

$$\mathcal{J}_k = \tfrac{4}{3}\mathcal{J}_0 \sin^2\left(\gamma - \tfrac{2}{3}k\pi\right). \tag{2.3}$$

With this convention, the axes 1, 2, and 3 correspond to long (l), short (s), and intermediate (m) semiaxes of the ellipsoidal shape when $\gamma \in (60^\circ, 120^\circ)$. This choice of the γ domain assures that the third axis which will be further used as a quantization axis is the one favored by the core's rotation and always has the maximal MOI. The different alignments depend on the quasiparticle nature of the involved nucleons [11]. Thus, a hole will align its spin along the l axis, a particle along the s axis, while a nucleon from a half filled orbital aligns its spin along the m axis.

Using a time-dependent variational principle in conjunction with a SU(2) coherent state for the total angular momentum operators [51–53,60], one can define from H_{align} a classical energy function

$$\mathcal{H}(x, \varphi) = \mathcal{H}_I(x, \varphi) - \mathcal{H}_{Ij}^a(x, \varphi), \quad a = 1, 2, \tag{2.4}$$

where

$$\mathcal{H}_I(x, \varphi) = \frac{I}{2}(A_1 + A_2) + A_3 I^2 + \frac{(2I-1)(I^2 - x^2)}{2I}(A_1 \cos^2\varphi + A_2 \sin^2\varphi - A_3), \tag{2.5}$$

$$\mathcal{H}_{Ij}^1(x, \varphi) = 2\sqrt{I^2 - x^2} A_1 j \cos\varphi, \tag{2.6}$$

$$\mathcal{H}_{Ij}^2(x, \varphi) = 2\sqrt{I^2 - x^2} A_2 j \sin\varphi \tag{2.7}$$

are functions of the azimuth angle φ and of the projection $x = I\cos\theta$ on the third axis of the total angular momentum vector. The two variables are canonical conjugates, φ being thus a generalized coordinate, while x a generalized momentum [53,60–62]. The case of an alignment along the medium axis must be treated separately because it coincides with the quantization axis. In this situation one cannot treat properly the fluctuation of the angular momentum vector with the restraint $|x| \leqslant I$ used to parametrize the coherent state. One option is to relabel the axes by rotating the variational function as in Ref. [51]. Another option is to redefine the x variable with a shift in the domain of values for the polar angle. Here, we use the results (2.6) and (2.7) simply in a different interval of the triaxial deformation, which makes the alignment to be along a medium intrinsic axis. This is, e.g., achieved in the

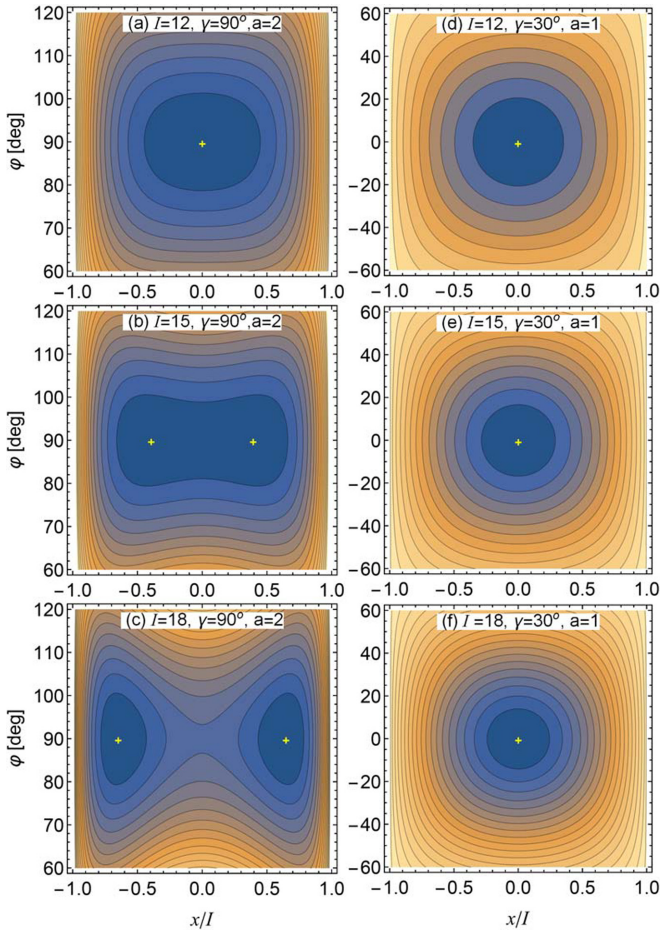

FIG. 1. Classical energy surfaces for $j = 10$ and different values of total angular momentum, as a function of φ and x when $\gamma = 90°$, $a = 2$ (left column, pair alignment along short axis) and $\gamma = 30°$, $a = 1$ (right column, pair alignment along medium axis). The single or double minima are indicated with crosses, while the difference between two contour lines is 7 units of $1/\mathcal{J}_0$ for the left column and 25 $1/\mathcal{J}_0$ units for the right column.

$\gamma \in (0, 60°)$ interval, where axis 1 becomes the medium axis and has the maximum MOI.

The evolution with angular momentum of the classical energy surface for the two distinct alignment cases is shown in Fig. 1. In the first rotational regime, where the alignment is perpendicular to the axis with maximal MOI, the classical energy function has a single minimum which gradually splits in two as the angular momentum increases. The same phenomenon is reported in diverse approaches [17,29,30,35,36], where however the polar and azimuth angles are independent coordinates. Such a behavior is shown in Figs. 1(a)–1(c) for short axis alignment. The long axis alignment situation is similar but with a 90° shift in the position of φ. The single minimum phase before the bifurcation corresponds to the transverse regime [10,11] with an unexpected rotation of the system around a principal axis whose MOI is not the maximal one. The system tends to re-establish the natural rotation around the axis with the maximal MOI, hence the emergence of two minima which move asymptotically

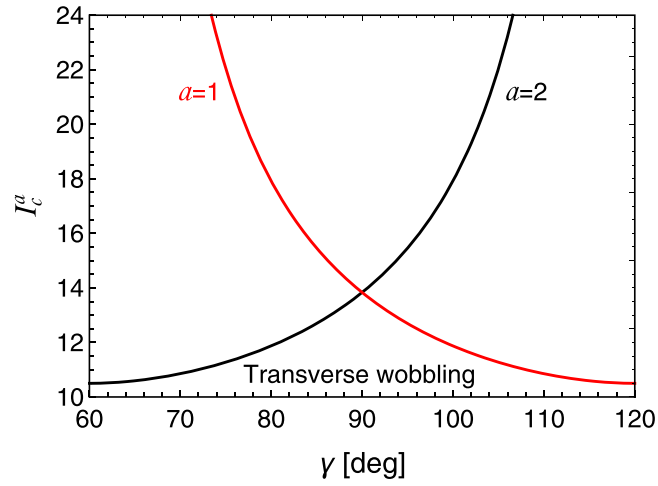

FIG. 2. The evolution with triaxial deformation of the classical critical angular momentum which delimits the transverse wobbling regime from the tilted-axis regime with double minima in the classical energy function of the assumed FA geometry along first ($a = 1$) and second ($a = 2$) principal axes.

towards the positive or negative values on the medium axis as angular momentum increases. The softening of the transverse wobbling and its ulterior transition towards a tilted axis rotation was first discussed within a cranking model with RPA [63], where the mechanism was investigated as a function of triaxial deformation. In the present formalism, the critical angular momentum where the classical energy function acquires two minima also depends on the triaxial deformation and the involved alignment as follows:

$$I_c^a = \frac{A_a j}{(A_a - A_3)} + \frac{1}{2}, \quad a = 1, 2. \tag{2.8}$$

Its dependence on triaxiality is depicted in Fig. 2. At $\gamma = 90°(A_1 = A_2)$, the critical angular momentum for alignment along axes 1 and 2 is the same. Nevertheless, decreasing triaxiality towards prolate shapes $\gamma > 90°$ extends the transverse phase to higher angular momentum states when the alignment is along axis 2 (s), and lowers its domain of existence when the alignment is along axis 1 (l). This result is especially important for the targeted $A \approx 130$ region of the nuclide chart, where one can have bands built on $h_{11/2}$ proton particles as well as $h_{11/2}$ neutron holes [45,48,49].

When the alignment is along the m axis with the largest MOI, the classical energy function shown in the Figs. 1(d)–1(f), exhibits a single deep minimum corresponding to the most favorable direction of the total angular momentum vector. The minimum deepens when the angular momentum increases. It reminds of the rotation of the usual triaxial rigid rotor [2], and therefore is referred to as longitudinal phase.

A quantum Hamiltonian can be obtained from the classical energy by a correspondence principle between the canonical variables and their operator realizations. This is achieved by performing first a harmonic approximation on the variable which exhibits a single minimum in the classical energy function. In this way one retains all the information regarding the other variable responsible for the system's dynamics. The

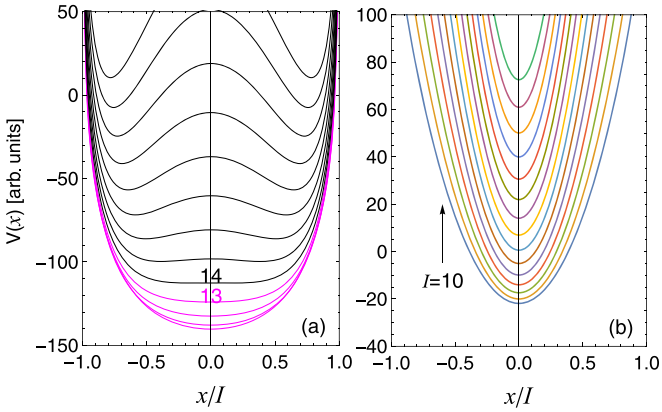

FIG. 3. The quantum wobbling potential as a function of the projection variable x, for different values of the total angular momentum and the following alignment geometries: (a) $\gamma = 90^\circ$, $j = 10$, and $a = 2$. The transition from a single minimum (transverse wobbling) to double minima (tilted-axis wobbling) is noted by change of color; (b) $\gamma = 30^\circ$, $j = 10$, and $a = 1$.

chosen geometries in this study lead to a classical energy function which always has a single minimum along the azimuth angle φ. A harmonic expansion in this variable is then a sensible approximation for the classical energy function:

$$\tilde{\mathcal{H}}(x,\varphi) \approx \mathcal{H}(x,\varphi_0) + \frac{1}{2}\left(\frac{\partial^2 \mathcal{H}}{\partial \varphi^2}\right)_{\varphi_0} (\varphi - \varphi_0)^2, \tag{2.9}$$

where the φ_0 minimizes the classical energy function for any x. In contradistinction to chiral geometry [60–62], φ_0 is a constant here, having the value 90° for alignment along axis 2 (s) when $\gamma \in (60^\circ, 120^\circ)$ and the value 0 for alignment along axis 1 when it is medium for $\gamma \in (0^\circ, 60^\circ)$ and long for $\gamma \in (60^\circ, 120^\circ)$. The quantization of the approximated energy function (2.9) is realized then in the momentum space of the projection variable x, by the simple replacement $\varphi - \varphi_0 = i\frac{d}{dx}$. Then the quantum energies are obtained from the Hamiltonian

$$\hat{H}_c = -\frac{1}{2}\frac{1}{\sqrt{B(x)}}\frac{d}{dx}\frac{1}{\sqrt{B(x)}}\frac{d}{dx} + V(x), \tag{2.10}$$

where

$$B(x) = \left[\frac{\partial^2 \mathcal{H}(x,\varphi)}{\partial \varphi^2}\right]^{-1}_{\varphi_0}, \tag{2.11}$$

$$V(x) = \mathcal{H}(x,\varphi_0) + \frac{B''(x)}{8[B(x)]^2} - \frac{9[B'(x)]^2}{32[B(x)]^3} \tag{2.12}$$

are the coordinate-dependent effective mass and the wobbling potential. As can be seen from Fig. 3, the wobbling potential follows the characteristics of the original classical energy function. Indeed, for the case with transverse alignment the wobbling potential exhibits the same transition from a single to double symmetric minima. A similar behavior was found in the potential of the wobbling collective Hamiltonian discussed in Refs. [29,30]. For the longitudinal alignment, the potential presents a single minimum with an increasing confinement with total angular momentum.

The quantum Hamiltonian is diagonalized in a basis of particle in the box wave functions, because the problem is naturally bounded by $|x| \leqslant I$. The wave function determined from the diagonalization procedure $F_{Is}(x)$ is used to define the coefficients

$$A_{IKp} = \left[\sum_{K=-I}^{I} F_{Ip}(K)^2\right]^{-1/2} F_{Ip}(K) \tag{2.13}$$

of the total wave function

$$|\Psi_{IMp}\rangle = \sum_{K=-I}^{I} A_{IKp}|IKM\rangle. \tag{2.14}$$

This wave function with p indexing the solutions of the Hamiltonian (2.10) is then used to calculate electromagnetic transitions. To do this, we use for the $E2$ transition operator, its second order expansion [64,65]

$$T_{2\mu}(E2) = t_1 q_{2\mu} + t_2[q \times q]_{2\mu}, \tag{2.15}$$

in quadrupole moments

$$q_{2\mu} = \beta\left[\cos\gamma D^2_{\mu 0} + \frac{\sin\gamma}{\sqrt{2}}\left(D^2_{\mu 2} + D^2_{\mu -2}\right)\right]. \tag{2.16}$$

It is worth mentioning that the $E2$ operator form (2.15) is an indispensable element of the interacting boson approximation [66]. Using the expression for the second order term [64,67], one can write the $E2$ operator as

$$T_{2\mu}(E2) = \sqrt{\frac{5}{16\pi}}\left[\tilde{Q}_0 D^2_{\mu 0} + \frac{\tilde{Q}_2}{\sqrt{2}}\left(D^2_{\mu 2} + D^2_{\mu -2}\right)\right]. \tag{2.17}$$

The redefined quadrupole components are

$$\tilde{Q}_0 = Q\left(\cos\gamma - \chi\beta\sqrt{\frac{2}{7}}\cos 2\gamma\right),$$
$$\tilde{Q}_2 = Q\left(\sin\gamma + \chi\beta\sqrt{\frac{2}{7}}\sin 2\gamma\right), \tag{2.18}$$

where Q is an empirical quadrupole moment value, β is the quadrupole deformation, while χ is an adjustable parameter of the relative contribution of the two terms from Eq. (2.15). The relevant expression of the $M1$ transition operator can be expressed as

$$T_{1\mu}(M1) = \sqrt{\frac{3}{4\pi}}\mu_N g_{\text{eff}} \sum_{\nu=0,\pm 1} j_\nu D^1_{\mu\nu}, \tag{2.19}$$

where $g_{\text{eff}} = g_j - g_R$ is an effective gyromagnetic factor. The final formulas for the $E2$ and $M1$ transition probabilities are straightforward, with the stipulation that for the $B(M1)$ the eigenvalues of the spherical components of the quasiparticle spin operators are approximated to values consistent with FA.

At this point it is opportune to discuss the particular characteristics of the present model in comparison to the traditional PRM calculations and other alternative approaches. The model basically combines the advantages of both PRM and TAC approaches. On one hand, it is based on the quantum structure of the PRM Hamiltonian. On the other hand it ascribes to it a classical dynamical description in terms of the directional angles of the total angular momentum vector

which is constrained as in TAC by the rigid quasiparticle alignments. Of course one has the FA approximation to keep the problem tractable, which at first seems as a drastic approximation. Nevertheless, the recent analysis of the PRM results through semiclassical spin coherent state maps showed that the probability distribution of the quasiparticle alignment vector remains unchanged for an extended interval of lower total angular momentum values [19]. At higher spins, in the vicinity and beyond the transversal wobbling critical point, it has a different structure but its highest probability is still closest to the original principal axis alignment. Moreover, the PRM results within the weak coupling basis [17] showed that the rotor angular momentum follows closely the evolution of the total angular momentum vector presented here, demonstrating thus that the major dynamical features of the systems are determined by the core's degrees of freedom and that FA is a suitable approximation. Note also that the rigid alignment of quasiparticles cannot be achieved in PRM due to the quantum fluctuation of the single particle spins, and therefore cannot be properly investigated and must not be discarded based on model-dependent criteria. While the PRM results offer an averaged dynamical picture as an output, the present model starts with it and one can therefore ascertain its validity when confronted with experimental data, as will be shown in the next section. Finally, it is worth to mention that in comparison to the present model, where the MOI are constant and of hydrodynamical nature, the reproduction of data within full PRM often requires cranking MOI [11] or an empirically induced spin-dependence of the scaling MOI $\mathcal{J}_0$ [14–16,18,20,22,34,37,39,46]. The later artifice is often overlooked, but it has a clear contamination effect on the spin dependence of the wobbling excitation energy which is the most important signature of the distinct wobbling modes.

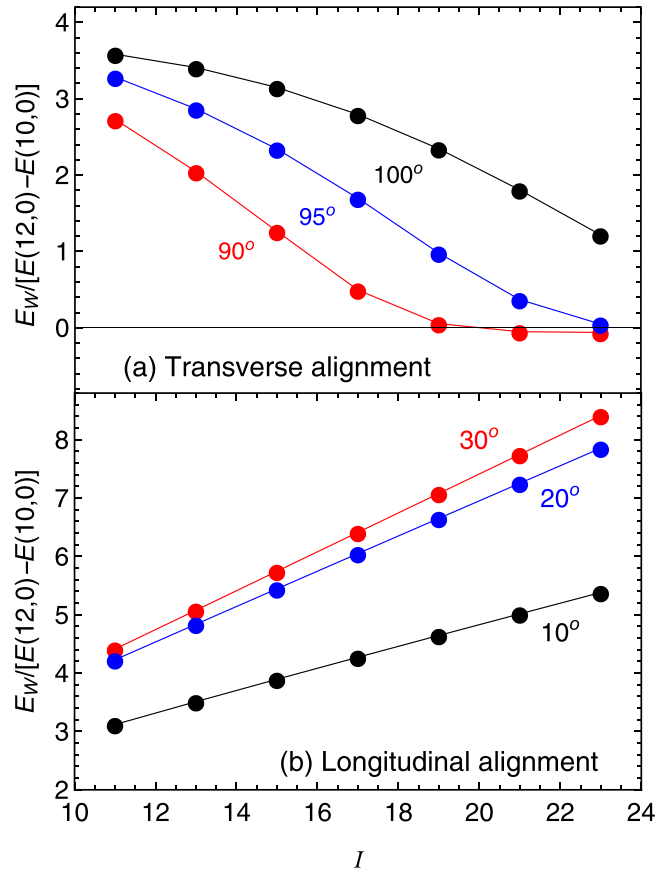

FIG. 4. Evolution with angular momentum of the transverse (a) and longitudinal (b) wobbling energy (3.2) normalized to a rotational excitation for few values of the triaxial deformation γ. The wobbling energy is calculated using only the diagonalization results for alignment $j = 10$ along axis 2(s), respectively, axis 1(m).

III. NUMERICAL APPLICATIONS

The final formula for the energy levels is

$$E(I,n) = E_{\rm diag}(\mathcal{J}_0,\gamma;Ip) + CI(I+1) + E_0, \qquad (3.1)$$

where the first term represents the energy determined from the diagonalization of Eq. (2.10) and depends only on the triaxial deformation γ and the scaling factor $1/\mathcal{J}_0$. n is the wobbling quantum number and its relationship with the solution index p is $n = p - 1$. The second term is a rotational correction which does not change the quantum system, the wave function being invariant to the $\hat{J}^2$ operator. Finally, E_0 is a reference energy. Even spins and $n = 0$ ($p = 1$) are considered for the yrast band and, respectively, odd spins and $n = 1$ ($p = 2$) for the excited band. The wobbling energy excitation is then defined as

$$E_W(I) = E(I,1) - \tfrac{1}{2}[E(I+1,0) + E(I-1,0)]. \qquad (3.2)$$

A simple calculus shows that the additional rotation term $CI(I+1)$ has just a constant contribution to the wobbling energy. Therefore, the wobbling energy effectively depends only on the triaxial deformation. A few samples of the angular momentum dependence of the wobbling energy are shown in Fig. 4(a) for few values of the triaxial deformation and alignment along the short axis. It reminds of the evolution with spin of the energy difference between chiral bands [60,61], which was also invoked previously in Refs. [53,68]. Before the critical angular momentum, the system's rotation axis has a regular fluctuation around the short axis consistent with the transverse wobbling. After the critical angular momentum, two nonaxial directions become energetically favorable, and the transverse regime transforms gradually first into a double-well vibration (energy above barrier) and then into a tunneling oscillation (energy below barrier). The loss of tunneling marks the installment of static tilted-axis configurations, and coincides with wobbling energy reaching a minimum limit defined only by the signature splitting of the rotational excitations. This change is obviously delayed when higher excited states with $n > 1$ are considered, because tunneling is still active. This aspect was used in Ref. [63] to advance the first signature for the transverse wobbling softening, based on the relative evolution with spin of the one and two phonon wobbling energies of the ^{163}Lu nucleus.

For the longitudinal alignment case we obtain an invariable linear angular momentum dependence of the wobbling energy. Figure 4(b) shows that the only obvious effect of a decreasing triaxiality is the decreasing magnitude of the wobbling excitations relative to the rotational ones.

TABLE I. The triaxiality γ with the parameters $\mathcal{J}_0$ [MeV^{-1}], E_0 [MeV], and C [keV] obtained by fitting the experimental excitation energies of ^{130}Ba, ^{134}Ce, and ^{136,138}Nd. The corresponding MOI in $\hbar^2$/MeV units obtained from Eq. (2.3) with the listed parameters, and the resulted classical value of the critical angular momentum are also given for reference.

Nucl.	γ	$\mathcal{J}_0$	E_0	C	$\mathcal{J}_{1(l)}$	$\mathcal{J}_{2(s)}$	$\mathcal{J}_{3(m)}$	I_c
^{130}Ba	101°	61.09	4.17	5.96	8.6	35.1	78.5	18.6
^{134}Ce	102°	61.95	3.54	8.45	7.9	37.0	79.0	19.3
^{136}Nd	97°	46.30	4.45	5.43	9.4	22.4	60.8	16.3
^{138}Nd	97°	47.59	4.49	7.96	9.7	23.0	62.5	16.3

The model contains four adjustable parameters, γ, $\mathcal{J}_0$, C, and E_0, with only two of them involved nonlinearly. Indeed, considering excitation energies in reference to the 10^+ level, one can drop the E_0 parameter. Similarly, normalizing the obtained excitation energies to an arbitrary excitation energy, say $E(12^+) - E(10^+)$, one will arrive at quantities which depend only on γ and the relative contribution $C\mathcal{J}_0$. These two measures represent the intrinsic parameters of the model, completely determining its spectral characteristics up to a scaling factor. Nevertheless, for a more direct comparison to experimental data we adjust all four parameters.

The wobbling bands identified so far in the ^{130}Ba, ^{134}Ce, and ^{136,138}Nd are built on a $\pi h^2_{11/2}$ quasiparticle configuration and therefore the model is considered with an alignment along the second axis (s). The parameters defining the total energy in Eq. (3.1), are obtained by minimizing the sum of the root mean square values corresponding to the wobbling energy, and the energies of the levels in the yrast and one-phonon wobbling bands. In this way, a well balanced fitting procedure is assured because the excitation energies of the rotational states are on average three times larger and can thus dominate the fit in detriment of wobbling effects. The fits are performed for energy levels up to the highest experimentally observed states connected through the relation (3.2). Thus one can ascertain by extrapolation if other members of one of the two considered bands conforms with the present wobbling model. Although both bands of ^{130}Ba are quite extended, one limits the fitting procedure for this nucleus up to $I = 24$, beyond which the structure of the bands significantly changes and the wobbling picture is no longer valid. The resulted parameters are listed in Table I, along with other relevant structural quantities. As can be attested by the graphs of Fig. 5, the agreement between experiment and theoretical calculations is quite good.

The triaxiality of the ^{136,138}Nd nuclei is found to be larger (closer to maximal 90° triaxiality) than for the other two nuclei which have a more axially symmetric shape. ^{130}Ba and ^{134}Ce exhibit a similar behavior in what concerns the energy levels and wobbling energy. A change in the rotational behavior as in the $I > 24$ states of ^{130}Ba is observed also in the yrast band of ^{134}Ce but earlier by few units of angular momentum. Therefore, its wobbling behavior is justified only for a few angular momentum states. The moderate triaxiality of ^{130}Ba and almost maximal triaxiality of ^{136}Nd are in agreement with calculations made in Refs. [45,47]. This implies a shorter spin interval for the existence of the transverse wobbling regime in Nd nuclei, confirmed by the classical critical angular momenta listed in Table I. The effect of apparently small difference between the γ values of Nd isotopes and those of the other two nuclei is evident from the classical critical angular momenta listed in Table I and from Fig. 5, where the calculated splitting of the bands is maintained significantly longer for ^{130}Ba and ^{134}Ce. The premature ending of the transverse regime in Nd nuclei, also suggests that it can also rapidly reach the regime of static tilted-axis rotation where the two wobbling bands merge into a single $\Delta I = 1$ regular sequence. Figures 5(c) and 5(d) shows that this happens at $I = 24$, and that the higher spin states observed in the yrast bands conform very well to this behavior.

It must be mentioned that the theoretical results for the ^{136}Nd nucleus were recently used as a supporting factor for the wobbling interpretation of the new experimental data reported in Ref. [69]. The above discussion then serves as a useful complement for the understanding of the wobbling features of this nucleus.

As can be inferred from Fig. 2, the high triaxiality of the Nd nuclei can sustain a transverse regime also built on an alignment of holes along the long axis, but for a much shorter range of spins due to $I_c = 12.3$. This hypothesis is checked by extrapolating the theoretical results for the $\pi h^2_{11/2}$ bands of ^{138}Nd to the bands L6 and L7 reported in Ref. [50] as being based on a $\nu h^{-2}_{11/2}$ configuration. This is achieved only by adjusting $E_0 = 7.33$, which is consistent with the different rotational contribution $A_{1,2}j^2$ of the pair. As can be seen in Fig. 6, this extrapolation excellently reproduces the first few low-lying states of the yrast band and the general energy elevation of the excited band. The present results reaffirms the conclusions of the RPA calculations performed in Ref. [50], that the L6 and L7 bands of ^{138}Nd can be interpreted in terms of wobbling excitations, albeit with important anharmonicities. Note however, that the experimental excited band has a strikingly different behavior of the rotational sequence [50], as opposing to the theoretical results and the behavior shown in Fig. 5, which suggests a different effective rotational inertia relative to the yrast band. Nevertheless, the results of Fig. 6 provides the first possible experimental realization of transverse wobbling constructed on hole alignments and supports the correct determination of the triaxial deformation of ^{138}Nd from the $\pi h^2_{11/2}$ bands.

For the calculation of $E2$ transition probabilities, one uses the available experimental data to fit the additional parameter χ. Extensive data are available only for the ^{130}Ba nucleus, for which we performed calculations considering $\beta = 0.195$ adopted from [70] in Eqs. (2.18). The obtained value of $\chi = 3.14$ is in a general good agreement with expected relative contributions [65,67] of the two terms from Eq. (2.15). The theoretical calculations for ^{130}Ba shown in Table II can be considered as an acceptable reference for ^{134}Ce predictions, given their similar deformation. Comparing in Table II the theoretical to the experimental values for the $B(E2)_{\text{out}}/B(E2)_{\text{in}}$ ratios, one can see that most theoretical values are within the error bars of the corresponding experimental ones, with the

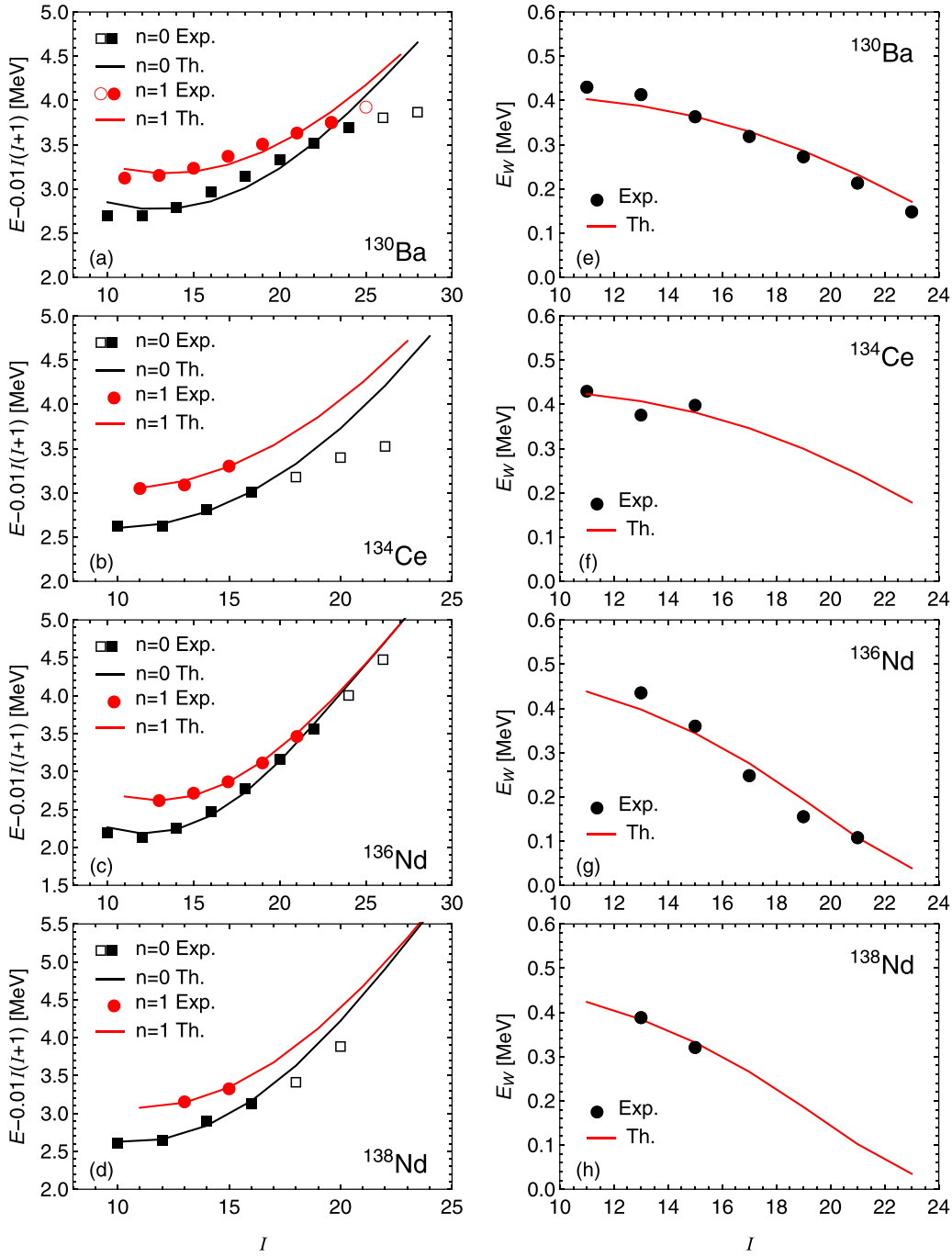

FIG. 5. Calculated energies (minus a common rigid-rotor reference) of the yrast and excited bands for ^{130}Ba, ^{134}Ce, and ^{136,138}Nd, are compared to experimental data in the left column. Open symbols designate data points which were not considered in the fitting procedure. The corresponding theoretical and experimental wobbling energies are compared in the right column.

exception of the transition from the $I = 21$ state, which is underestimated. From the renormalized quadrupole components (2.18), we can extract an effective triaxial deformation as $\tan\gamma_{\rm eff} = \tilde{Q}_2/\tilde{Q}_0$. The values 83° and 85° obtained for ^{130}Ba and ^{136}Nd respectively, are on the oblate side and lead to an inverted $\mathcal{J}_1 > \mathcal{J}_2$ relationship. This inconsistency was also reported in Ref. [55].

The other usually sought $B(M1)_{\rm out}/B(E2)_{\rm in}$ ratio is unfortunately factorized by the quantity $(g_{\rm eff}/Q)^2$ involving subjective assumptions. For example, the usual quenching of the free spin gyromagnetic factor and the crude hydrodynamic estimation of Q lead to theoretical $B(M1)_{\rm out}/B(E2)_{\rm in}$ ratios which overestimate the experimental values by one order of magnitude. Alternative quenching mechanisms [37,53,55] are usually adopted in order to match the experimental values and which in principle can account for the missing effects such as, e.g., the coupling of the wobbling and scissor-like excitations [28]. We chose here to fix the quantity $g_{\rm eff}/Q$ by fitting the

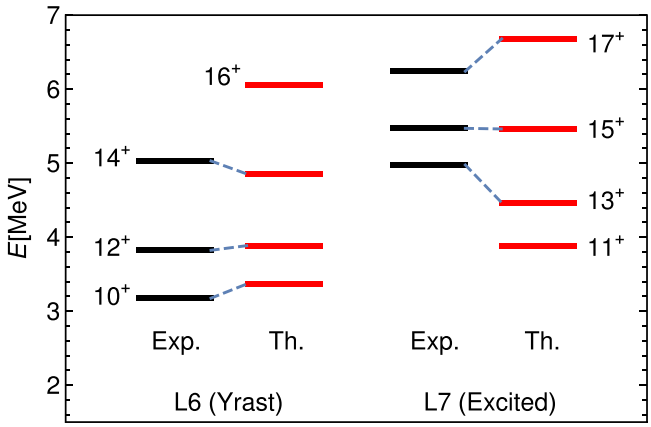

FIG. 6. Comparison between experimental [50] and predicted energies of the yrast band (L6) and excited band (L7) of ^{138}Nd.

experimental $\Delta I = 1$ mixing ratios which usually accompany the data on $B(M1)_{\rm out}/B(E2)_{\rm in}$ with the theoretical formula [71]. The experimental and predicted values for both mixing and $B(M1)_{\rm out}/B(E2)_{\rm in}$ ratios are listed in Table II for ^{130}Ba. The theoretical values reproduce the correct experimental behavior of δ as well as $B(M1)_{\rm out}/B(E2)_{\rm in}$. This includes the increase of the later at high spin, an aspect which was not reproduced by the PRM calculations performed in Ref. [46].

TABLE II. Experimental and theoretical mixing ratios $\delta_{I\to I-1}$, transition probability ratio $B(M1)_{\rm out}/B(E2)_{\rm in}$ in $(\mu_N/eb)^2$ units and the dimensionless $B(E2)_{\rm out}/B(E2)_{\rm in}$ ratio, between the excited and yrast quasiparticle bands of ^{130}Ba [45,46].

	δ		$\frac{B(M1)_{\rm out}}{B(E2)_{\rm in}}$		$\frac{B(E2)_{\rm out}}{B(E2)_{\rm in}}$	
I	Exp.	Th.	Exp.	Th.	Exp.	Th.
13	−0.58(13)	−0.59	0.36^{+19}_{-13}	0.34	0.32^{+18}_{-15}	0.39
15	−0.62(10)	−0.61	0.38^{+61}_{-16}	0.31	0.36^{+70}_{-19}	0.33
17	−0.62(10)	−0.62	0.23^{+22}_{-9}	0.30	0.22^{+27}_{-10}	0.29
19	−0.60	−0.61	0.25^{+23}_{-8}	0.29	0.22^{+21}_{-7}	0.25
21	−0.60	−0.59	0.43^{+35}_{-13}	0.30	0.41^{+34}_{-13}	0.23
23		−0.55		0.33		0.22

IV. CONCLUSIONS

The dynamical features of a nuclear system composed of a triaxial core and a rigidly aligned pair of quasiparticles are investigated in a semiclassical approach. The main result of the present study refers to the construction of a Schrödinger equation for a variable associated with the angular momentum projection, whose potential retains the maximal information regarding its wobbling motion. The model is successfully applied for the description of wobbling excitations proposed in the two-quasiproton bands of ^{130}Ba, ^{134}Ce, and ^{136,138}Nd. Moreover, the extension of the corresponding model calculations to the two-neutron hole bands from ^{138}Nd, supports their earlier wobbling interpretation [50].

As a future application of the proposed model, we intend a revisiting of the wobbling excitations in odd mass nuclei. While for its further development, one plans the introduction of a tilt in the frozen alignment for a more realistic representation of the quasiparticles which are generally not of pure hole or particle nature and therefore are not perfectly aligned to the body-fixed principal axes. This extension is expected to describe a true tilted-axis wobbling motion.

ACKNOWLEDGMENT

This work was supported by a grant of the Ministry of Research, Innovation and Digitalization, CNCS - UEFISCDI, Project No. PN-III-P1-1.1-TE-2021-0109, within PNCDI III.

[1] A. S. Davydov and G. F. Filippov, Nucl. Phys. **8**, 237 (1958).
[2] A. Bohr and B. R. Mottelson, *Nuclear Structure*, Vol. 2 (Benjamin, Reading, MA, 1975).
[3] B. Qi, H. Zhang, S. Y. Wang, and Q. B. Chen, J. Phys. G: Nucl. Part. Phys. **48**, 055102 (2021).
[4] H. Schnack-Petersen *et al.*, Nucl. Phys. A **594**, 175 (1995).
[5] S. W. Ødegård, G. B. Hagemann, D. R. Jensen, M. Bergström, B. Herskind, G. Sletten, S. Törmänen, J. N. Wilson, P. O. Tjøm, I. Hamamoto, K. Spohr, H. Hübel, A. Görgen, G. Schönwasser, A. Bracco, S. Leoni, A. Maj, C. M. Petrache, P. Bednarczyk, and D. Curien, Phys. Rev. Lett. **86**, 5866 (2001).
[6] P. Bringel *et al.*, Eur. Phys. J. A **24**, 167 (2005).
[7] G. Schönwaßer *et al.*, Phys. Lett. B **552**, 9 (2003).
[8] H. Amro *et al.*, Phys. Lett. B **553**, 197 (2003).
[9] D. J. Hartley, R. V. F. Janssens, L. L. Riedinger, M. A. Riley, A. Aguilar, M. P. Carpenter, C. J. Chiara, P. Chowdhury, I. G. Darby, U. Garg, Q. A. Ijaz, F. G. Kondev, S. Lakshmi, T. Lauritsen, A. Ludington, W. C. Ma, E. A. McCutchan, S. Mukhopadhyay, R. Pifer, E. P. Seyfried, I. Stefanescu, S. K. Tandel, U. Tandel, J. R. Vanhoy, X. Wang, S. Zhu, I. Hamamoto, and S. Frauendorf, Phys. Rev. C **80**, 041304(R) (2009).
[10] Y. R. Shimizu, M. Matsuzaki, and K. Matsuyanagi, arXiv:nucl-th/0404063.
[11] S. Frauendorf and F. Dönau, Phys. Rev. C **89**, 014322 (2014).
[12] I. Hamamoto, Phys. Rev. C **65**, 044305 (2002).
[13] I. Hamamoto and G. B. Hagemann, Phys. Rev. C **67**, 014319 (2003).
[14] K. Tanabe and K. Sugawara-Tanabe, Phys. Rev. C **95**, 064315 (2017).
[15] K. Sugawara-Tanabe and K. Tanabe, Phys. Scr. **92**, 094005 (2017).
[16] K. Sugawara-Tanabe and K. Tanabe, Phys. Rev. C **82**, 051303(R) (2010).
[17] E. Streck, Q. B. Chen, N. Kaiser, and Ulf-G. Meißner, Phys. Rev. C **98**, 044314 (2018).
[18] C. Broocks, Q. B. Chen, N. Kaiser, and G. Meißner, Eur. Phys. J. A **57**, 161 (2021).
[19] Q. B. Chen and S. Frauendorf, Eur. Phys. J. A **58**, 75 (2022).
[20] H. Zhang, B. Qi, X. D. Wang, H. Jia, and S. Y. Wang, Phys. Rev. C **105**, 034339 (2022).
[21] S. Frauendorf, Nucl. Phys. A **557**, 259c (1993).
[22] J. T. Matta, U. Garg, W. Li, S. Frauendorf, A. D. Ayangeakaa, D. Patel, K. W. Schlax, R. Palit, S. Saha, J. Sethi, T. Trivedi,

S. S. Ghugre, R. Raut, A. K. Sinha, R. V. F. Janssens, S. Zhu, M. P. Carpenter, T. Lauritsen, D. Seweryniak, C. J. Chiara, F. G. Kondev, D. J. Hartley, C. M. Petrache, S. Mukhopadhyay, D. V. Lakshmi, M. K. Raju, P. V. MadhusudhanaRao, S. K. Tandel, S. Ray, and F. Donau, Phys. Rev. Lett. **114**, 082501 (2015).

[23] M. Matsuzaki, Y. R. Shimizu, and K. Matsuyanagi, Phys. Rev. C **65**, 041303(R) (2002).

[24] M. Matsuzaki, Y. R. Shimizu, and K. Matsuyanagi, Eur. Phys. J. A **20**, 189 (2003).

[25] M. Matsuzaki, Y. R. Shimizu, and K. Matsuyanagi, Phys. Rev. C **69**, 034325 (2004).

[26] Y. R. Shimizu, T. Shoji, and M. Matsuzaki, Phys. Rev. C **77**, 024319 (2008).

[27] T. Shoji and Y. R. Shimizu, Prog. Theor. Phys. **121**, 319 (2009).

[28] S. Frauendorf and F. Dönau, Phys. Rev. C **92**, 064306 (2015).

[29] Q. B. Chen, S. Q. Zhang, P. W. Zhao, and J. Meng, Phys. Rev. C **90**, 044306 (2014).

[30] Q. B. Chen, S. Q. Zhang, and J. Meng, Phys. Rev. C **94**, 054308 (2016).

[31] X. H. Wu, Q. B. Chen, P. W. Zhao, S. Q. Zhang, and J. Meng, Phys. Rev. C **98**, 064302 (2018).

[32] J. A. Sheikh, G. H. Bhat, W. A. Dar, S. Jehangir, and P. A. Ganai, Phys. Scr. **91**, 063015 (2016).

[33] M. Shimada, Y. Fujioka, S. Tagami, and Y. R. Shimizu, Phys. Rev. C **97**, 024318 (2018).

[34] N. Sensharma *et al.*, Phys. Lett. B **792**, 170 (2019).

[35] Y. K. Wang, F. Q. Chen, and P. W. Zhao, Phys. Lett. B **802**, 135246 (2020).

[36] F.-Q. Chen and C. M. Petrache, Phys. Rev. C **103**, 064319 (2021).

[37] J. Timár, Q. B. Chen, B. Kruzsicz, D. Sohler, I. Kuti, S. Q. Zhang, J. Meng, P. Joshi, R. Wadsworth, K. Starosta, A. Algora, P. Bednarczyk, D. Curien, Z. Dombradi, G. Duchene, A. Gizon, J. Gizon, D. G. Jenkins, T. Koike, A. Krasznahorkay, J. Molnar, B. M. Nyako, E. S. Paul, G. Rainovski, J. N. Scheurer, A. J. Simons, C. Vaman, and L. Zolnai, Phys. Rev. Lett. **122**, 062501 (2019).

[38] S. Nandi, G. Mukherjee, Q. B. Chen, S. Frauendorf, R. Banik, S. Bhattacharya, S. Dar, S. Bhattacharyya, C. Bhattacharya, S. Chatterjee, S. Das, S. Samanta, R. Raut, S. S. Ghugre, S. Rajbanshi, S. Ali, H. Pai, M. A. Asgar, S. Das Gupta, P. Chowdhury, and A. Goswami, Phys. Rev. Lett. **125**, 132501 (2020).

[39] S. Biswas *et al.*, Eur. Phys. J. A **55**, 159 (2019).

[40] N. Sensharma, U. Garg, Q. B. Chen, S. Frauendorf, D. P. Burdette, J. L. Cozzi, K. B. Howard, S. Zhu, M. P. Carpenter, P. Copp, F. G. Kondev, T. Lauritsen, J. Li, D. Seweryniak, J. Wu, A. D. Ayangeakaa, D. J. Hartley, R. V. F. Janssens, A. M. Forney, W. B. Walters, S. S. Ghugre, and R. Palit, Phys. Rev. Lett. **124**, 052501 (2020).

[41] S. Chakraborty *et al.*, Phys. Lett. B **811**, 135854 (2020).

[42] E. A. Lawrie, O. Shirinda, and C. M. Petrache, Phys. Rev. C **101**, 034306 (2020).

[43] B. F. Lv, C. M. Petrache, E. A. Lawrie, A. Astier, E. Dupont, K. K. Zheng, P. Greenlees, H. Badran, T. Calverley, D. M. Cox, T. Grahn, J. Hilton, R. Julin, S. Juutinen, J. Konki, J. Pakarinen, P. Papadakis, J. Partanen, P. Rahkila, P. Ruotsalainen, M. Sandzelius, J. Saren, C. Scholey, J. Sorri, S. Stolze, J. Uusitalo, B. Cederwall, A. Ertoprak, H. Liu, S. Guo, J. G. Wang, H. J. Ong, X. H. Zhou, Z. Y. Sun, I. Kuti, J. Timar, A. Tucholski, J. Srebrny, and C. Andreoiu, Phys. Rev. C **103**, 044308 (2021).

[44] K. Nomura and C. M. Petrache, Phys. Rev. C **105**, 024320 (2022).

[45] C. M. Petrache *et al.*, Phys. Lett. B **795**, 241 (2019).

[46] Q. B. Chen, S. Frauendorf, and C. M. Petrache, Phys. Rev. C **100**, 061301(R) (2019).

[47] B. F. Lv, C. M. Petrache, A. Astier, E. Dupont, A. Lopez-Martens, P. T. Greenlees, H. Badran, T. Calverley, D. M. Cox, T. Grahn, J. Hilton, R. Julin, S. Juutinen, J. Konki, M. Leino, J. Pakarinen, P. Papadakis, J. Partanen, P. Rahkila, M. Sandzelius, J. Saren, C. Scholey, J. Sorri, S. Stolze, J. Uusitalo, A. Herzan, B. Cederwall, A. Ertoprak, H. Liu, S. Guo, M.L. Liu, Y. H. Qiang, J. G. Wang, X. H. Zhou, I. Kuti, J. Timar, A. Tucholski, J. Srebrny, and C. Andreoiu, Phys. Rev. C **98**, 044304 (2018).

[48] C. M. Petrache and S. Guo, arXiv:1603.08247.

[49] C. M. Petrache, S. Guo, A. D. Ayangeakaa, U. Garg, J. T. Matta, B. K. Nayak, D. Patel, M. P. Carpenter, C. J. Chiara, R. V. F. Janssens, F. G. Kondev, T. Lauritsen, D. Seweryniak, S. Zhu, S. S. Ghugre, and R. Palit, Phys. Rev. C **93**, 064305 (2016).

[50] C. M. Petrache, S. Frauendorf, M. Matsuzaki, R. Leguillon, T. Zerrouki, S. Lunardi, D. Bazzacco, C. A. Ur, E. Farnea, C. RossiAlvarez, R. Venturelli, and G. deAngelis, Phys. Rev. C **86**, 044321 (2012).

[51] A. A. Raduta, R. Budaca, and C. M. Raduta, Phys. Rev. C **76**, 064309 (2007).

[52] R. Budaca, Phys. Rev. C **97**, 024302 (2018).

[53] R. Budaca, Phys. Rev. C **103**, 044312 (2021).

[54] A. A. Raduta, R. Poenaru, and L. Gr. Ixaru, Phys. Rev. C **96**, 054320 (2017).

[55] A. A. Raduta, R. Poenaru, and C. M. Raduta, Phys. Rev. C **101**, 014302 (2020).

[56] R. Poenaru and A. A. Raduta, Rom. J. Phys. **66**, 308 (2021).

[57] C. M. Raduta, A. A. Raduta, R. Poenaru, and Al. H. Raduta, J. Phys. G: Nucl. Part. Phys. **49**, 025105 (2022).

[58] N. Hamermesh, *Group Theory and Its Application to Physical Problems* (Dover Publications, New York, 1962).

[59] A. A. Raduta and R. Budaca, Phys. Rev. C **84**, 044323 (2011).

[60] R. Budaca, Phys. Rev. C **98**, 014303 (2018).

[61] R. Budaca, Phys. Lett. B **797**, 134853 (2019).

[62] R. Budaca, Phys. Lett. B **817**, 136308 (2021).

[63] M. Matsuzaki and S.-I. Ohtsubo, Phys. Rev. C **69**, 064317 (2004).

[64] M. A. Caprio and F. Iachello, Nucl. Phys. A **781**, 26 (2007).

[65] A. A. Raduta and P. Buganu, Phys. Rev. C **83**, 034313 (2011).

[66] F. Iachello and A. Arima, *The Interacting Boson Model* (Cambridge University Press, Cambridge, 1987).

[67] A. A. Raduta and P. Buganu, Phys. Rev. C **88**, 064328 (2013).

[68] A. A. Raduta, C. M. Raduta, and R. Poenaru, J. Phys. G: Nucl. Part. Phys. **48**, 015106 (2021).

[69] B. F. Lv, C. M. Petrache, R. Budaca, A. Astier, K. K. Zheng, P. Greenlees, H. Badran, T. Calverley, D. M. Cox, T. Grahn, J. Hilton, R. Julin, S. Juutinen, J. Konki, J. Pakarinen, P. Papadakis, J. Partanen, P. Rahkila, P. Ruotsalainen, M. Sandzelius, J. Saren, C. Scholey, J. Sorri, S. Stolze, J. Uusitalo, B. Cederwall, A. Ertoprak, H. Liu, S. Guo, J. G. Wang, H. J. Ong, X. H. Zhou, Z. Y. Sun, I. Kuti, J. Timar, A. Tucholski, J. Srebrny, and C. Andreoiu, Phys. Rev. C **105**, 034302 (2022).

[70] P. Möller, A. J. Sierk, T. Ichikawa, and H. Sagawa, At. Data Nucl. Data Tables **109–110**, 1 (2016).

[71] H. Toki and A. Faessler, Nucl. Phys. A **253**, 231 (1975).